Protein Expression and Purification 199 (2022) 106134

Contents lists available at ScienceDirect

Protein Expression and Purification

journal homepage: www.elsevier.com/locate/yprep

Recombinant AcnB, NrdR and RibD of *Acinetobacter baumannii* and their potential interaction with DNA adenine methyltransferase AamA

Kristin Weber [a], Joerg Doellinger [b], Cy M. Jeffries [c], Gottfried Wilharm [a,*]

[a] Robert Koch Institute, Project Group P2 (Acinetobacter baumannii - Biology of a Nosocomial Pathogen), Burgstr. 37, 38855 Wernigerode, Germany
[b] Robert Koch Institute, Centre for Biological Threats and Special Pathogens, ZBS 6 (Proteomics and Spectroscopy); Seestr. 10, 13353, Berlin (Wedding), Germany
[c] European Molecular Biology Laboratory (EMBL), Svergun Group (Small-angle X-ray Scattering from Macromolecular Solutions), Notkestr. 85, Geb. 25a, 22607, Hamburg, Germany

ARTICLE INFO

Keywords:
AcnB
NrdR
RibD
AamA
Acinetobacter baumannii
DNA-Adenine-methyltransferase
Recombinant production
Small-angle X-ray scattering
SAXS
Solution structure

ABSTRACT

In the last decades *Acinetobacter baumannii* developed into an increasingly challenging nosocomial pathogen. *A. baumannii* ATCC 17978 harbors a DNA-(adenine N6)-methyltransferase termed AamA. Previous studies revealed a low specific activity of AamA *in vitro* despite proven folding, which led us to speculate about possible interaction partners assisting AamA in targeting methylation sites. Here, applying a pulldown assay with subsequent mass spectrometry we identified aconitate hydratase 2 (AcnB) as possible interaction partner. In addition, we considered the putative transcriptional regulator gene *nrdR* (A1S_0220) and the pyrimidine deaminase/reductase gene *ribD* (A1S_0221) of *A. baumannii* strain ATCC 17978 to encode additional potential interaction partners due to their vicinity to the *aamA* gene (A1S_0222). Proteins were recombinantly produced in the milligram scale, purified to near homogeneity, and interactions with AamA were studied applying blue native gel electrophoreses, electrophoretic mobility shift assay, chemical cross-linking and co-immunoprecipitation. These analyses did not provide evidence of interaction between AamA and purified proteins. Solution structures of RibD, NrdR and AcnB were studied by small-angle X-ray scattering (SAXS) alone and in combination with AamA. While in the case of RibD and AcnB no evidence of an interaction with AamA was produced, addition of AamA to NrdR resulted in dissociation of long and rod-shaped polymeric NrdR structures, implying a specific but transient interaction. Moreover, we identified a molecular crowding effect possibly impeding the DNA methyltransferase activity *in vivo* and a sequence-independent DNA binding activity of AamA calling for continued efforts to identify the interaction network of AamA.

1. Introduction

Bacteria hold restriction modification (R-M) systems which enable them to discriminate between own and foreign DNA. By marking the target DNA bases adenine (N-6) or cytosine (N-4, C-5) with a methyl group from S-adenosyl-methionine (SAM), cleavage of their own DNA through an associated cognate restriction endonuclease can be prevented. Methyltransferases like Dam of *E. coli* or CcrM of *Caulobacter crescentus* lacking such corresponding restriction enzymes, are called "orphan". Many of these orphan methyltransferases play an important role in regulatory processes such as transcription or replication. CcrM for example is a **c**ell-**c**ycle **r**egulated **m**ethyltransferase. The recognition sequence of this methyltransferase is GANTC where the adenine becomes methylated after replication. Besides importance of CcrM in cell cycle regulation, the methyltransferase is also essential for viability [1,2]. Another well-known representative of an orphan methyltransferase is the Dam methyltransferase of *E. coli*, a 32 kDa monomer recognizing GATC target sequences [3–5].

While screening a transposon mutant library looking for motility deficiencies, we identified a mutant of wildtype strain ATCC 17978 inactivated in gene *a1s_0222*, encoding a putative DNA (N-6-adenine) methyltransferase. Because it lacks an endonuclease activity, this methyltransferase termed AamA (***A**cinetobacter* **a**denine **m**ethyltransferase **A**) belongs to the group of "orphan" methyltransferases. AamA, a 49 kDa monomer, was recombinantly produced, purified and characterized [6]. Through Sanger sequencing, the DNA recognition and methylation site of AamA was identified as GAATTC, where the second adenine becomes methylated. The methyltransferase activity of AamA

* Corresponding author.
E-mail addresses: WeberK@rki.de (K. Weber), DoellingerJ@rki.de (J. Doellinger), cy.jeffries@embl-hamburg.de (C.M. Jeffries), WilharmG@rki.de (G. Wilharm).

https://doi.org/10.1016/j.pep.2022.106134
Received 2 June 2022; Received in revised form 17 June 2022; Accepted 20 June 2022
Available online 2 July 2022

was studied in a restriction-protection assay, and in comparison, to the commercially available *EcoRI* methyltransferase, showed a low specific activity *in vitro* despite proven folding. Although not previously reported for other DNA methyltransferases, this prompted us to speculate that AamA is supported by interaction partners during the methylation process, e.g., to guide AamA to designated methylation sites. In further support of this notion, AamA is significantly larger than Dam (49 kDa versus 32 kDa) allowing for additional functionality. In this paper we investigated the potential interaction between the recombinantly produced and purified partners AcnB, NrdR, RibD and AamA. Through a pulldown assay with subsequent mass spectrometry, AcnB was selected as a potential interaction partner. In addition, NrdR and RibD were selected and examined as potential interaction partners due to the proximity of encoding genes *nrdR* and *ribD* to the *aamA* gene. Until now only the structure of the pyrimidine deaminase/reductase (RibD) of *A. baumannii* strain ATCC 19606 was analyzed by Dawson et al. [7] but nothing is known about the putative transcriptional regulator NrdR and aconitate hydratase 2 (AcnB) and the potential of all three proteins to interact with AamA.

Below we point out general aspects of the potential interaction partners (NrdR, AcnB and RibD) of AamA.

NrdR from *Streptomyces coelicolor* was identified as a transcriptional regulator of class Ia and class II ribonucleotide reductases (RNRs) [8]. These enzymes play an important role in DNA synthesis because they provide the necessary deoxyribonucleotides for this process through ribonucleotide reduction. Beside oxygen-dependent (class I) and oxygen-independent (class II) RNRs also a third class mainly occurring in anaerobic bacteria is known. NrdR serves as a repressor by binding in the promotor-region of class I (*nrdABS*) and class II (*nrdRJ*) operons to prevent transcription of genes. These recognition sites along the DNA were named as NrdR box [9]. NrdR from *S. coelicolor* was recombinantly produced and purified and occurred in a monomer (22.1 kDa) and dimer form [8]. In addition, biochemical analysis revealed NrdR as a Zn ribbon/ATP cone protein. Through DNA-protein binding assays NrdR binding to DNA regions within the promotor regions of *nrdABS* or *nrdRJ* genes could be demonstrated [10]. In an adherent-invasive *E. coli* strain, NrdR showed a regulatory effect on motility and chemotaxis [11].

The bifunctional aconitate hydratase 2/2-metyhlisocitrate dehydratase (AcnB) is an iron-sulfur (4Fe–4S) protein which plays an important role in various metabolic pathways like tricarboxylic acid (TCA) cycle, glyoxylate cycle and glycolytic pathway. While *M. tuberculosis* carries only one *acn* gene, other bacteria like *E. coli* exhibit the isoforms AcnA and AcnB. In *A. baumannii* ATCC 17978 the aconitate hydratase 2/2-methylisocitrate dehydratase is encoded by the *acnB* gene (KEGG orthology-K01682). In the TCA cycle, AcnB is the predominant enzyme catalyzing the conversion of citrate into isocitrate through the intermediate *cis*-aconitate. Under certain environmental conditions like iron deficiency or oxidative stress caused through superoxide, nitric oxide or H_2O_2, AcnA is induced. As a consequence, AcnA and AcnB apo-proteins (iron-regulatory proteins-IRPs) having an RNA binding activity are formed by disassembling of the iron-sulfur cluster. Iron-responsive elements (IREs) along the mRNA are recognized through IRP and binding takes place at the 5′or 3′end of untranslated regions (UTRs) by forming stem loop structures. Depending on the RNA end the proteins are tied to, translation can be improved (3′UTRs) or inhibited (5 UTRs) [12–17]. The capability to target mRNA thereby regulating translation qualifies AcnB as a so-called moonlighting protein with more than one function.

Riboflavin (vitamin B2) is an essential precursor in the synthesis of the cofactors flavin adenine dinucleotide (FAD) and flavin mononucleotide (FMN) playing an important role in carbohydrate metabolism, energy production or as electron carrier in oxidation for example [18]. In the prokaryotic world, biosynthesis of riboflavin is best studied in the gram-positive bacterium *Bacillus subtilis*. Four genes termed *ribA* (encoding GTP cyclohydrolase/3,4-dihydroxy 2-butanone 4-phosphate (3,4-DHBP), *ribB* (encoding riboflavin synthase-α-chain), *ribG* (encoding pyrimidine deaminase/reductase) and *ribH* (encoding riboflavin synthase-β-chain) are concerted in the *rib* operon [19]. In *E. coli*, five genes responsible for riboflavin synthesis are known and scattered along the genome. In the latter species, GTP cyclohydrolase (RibA) and 3,4-dihydroxy 2-butanone 4-phosphate (RibB) are individually encoded by two genes. Furthermore, RibE and RibD of *E. coli* correspond to RibB and RibG of *B. subtilis* [20]. The structure of the bifunctional diaminohydroxyphosphoribosylaminopyrimidine deaminase/5-amino-6-(5-phosphoribosylamino) uracil reductase (RibD) of *A. baumannii* ATCC 19606 was analyzed through crystallization [7]. The structure of the *Ab*RibD subunit has a deaminase and reductase active site and a molecular mass of around 42 kDa [7].

Here, we used biochemical and biophysical methods to test on possible interactions of recombinantly produced and purified proteins AcnB, NrdR, and RibD with AamA.

2. Materials and methods

2.1. Pulldown assay

To identify potential protein interaction partners of AamA we first performed a pulldown assay. To this end, wildtype strain 29D2, the associated *aamA*$^-$ mutant (supplementation of 100 μg/ml kanamycin), *E. coli* BL21 (DE3) plysS pGEX-6P-3-GST (supplementation of 100 μg/ml ampicillin) and *E. coli* BL21 (DE3) plysS pGEX-6P-3-A1S_0222 (supplementation of 100 μg/ml ampicillin) were incubated over night at 37 °C in 3 ml Luria-Bertani (LB)-medium (10 g/L tryptone, 5 g/L yeast extract, 5 g/L NaCl, pH 7.4). The next day, cultures were diluted 1:100 in 200 ml fresh LB medium (supplemented with respective antibiotics) and grown in a 2 L bottle flask. Cultures of wildtype strain 29D2 and the associated *aamA*$^-$ mutant were again incubated over night at 37 °C. In the case of pGEX-6P-3-GST and pGEX-6P-3-A1S_0222, cultures were incubated for 5 h at 20 °C. After this time cultures were induced by 0.05 mM IPTG and were incubated for another 16 h at 20 °C. Next, all cultures were centrifuged (10,000×*g* for 20 min and 4 °C, rotor: 10-JA) and after a freezing step at −80 °C cells were resuspended in 20 ml cell disruption (CD)-buffer (300 mM NaCl, 5 mM EGTA (ethylene glycol-bis(2-aminoethylether)-N, N, N', N'-tetra-acetic acid), 1 mM EDTA (2, 2′, 2″, 2‴-(ethane-1,2-diyldinitrilo)-tetra-acetic acid), 1 mM DTT, 2 U Benzonase nuclease (250 U/μl), pH 7.4) and lysed with an Emulsiflex (Avestin). Afterwards the suspension was centrifuged twice (16,000×*g* for 25 min and 4 °C) and 0.1% Triton X-100 was added to GST/GST-AamA lysates. Until the bacterial lysates were used in the assay, they were stored at 4 °C or were frozen at −80 °C. In the meantime, the GST and GST-AamA proteins were purified using a GSTprep™ FF 16/10 column (20 ml bed volume). Therefore, the column first was equilibrated with 5 column volumes (CV) of GST binding buffer (300 mM NaCl, 1 mM EDTA, 5 mM EGTA, 5% glycerol, 1 mM DTT, pH 7.4) before proteins were loaded to the column. Afterwards, the column was washed with GST binding buffer again and proteins were eluted (300 mM NaCl, 50 mM Tris, 1 mM EDTA, 5 mM EGTA, 5% glycerol, 1 mM DTT, 10 mM reduced glutathione (GSH), pH 7.4). Samples were pooled after determination of protein amounts using Bradford reagent (GST/GST-AamA production and purification was performed and modified after Blaschke et al., 2018 [6]). To remove GSH, protein samples (GST/GST-AamA) were loaded on a PD-10 column. For equilibration of the column and elution of proteins the B1 buffer (150 mM NaCl, 10 mM Tris, 1 mM DTT, 5% glycerol) was used. Then, the Glutathione-Sepharose™ 4 Fast Flow (GE Healthcare; LOT: 10258578) resin was prepared according to manufacturer instructions. First, the bottle containing the resin was shaken very well and 200 μl slurry were taken out with a cropped pipette tip. After transfer to a 1.5 ml reaction tube the slurry was centrifuged at 500×*g* at 4 °C for 5 min. The supernatant was discarded. Then, the resin was washed twice with 1 ml of GST binding buffer, centrifuged (500×*g* for 5 min at 4 °C) and incubated for 15 min at 4 °C with 800 μg GST, 800 μg GST-AamA (fusion protein) or without (controls-included binding

buffer instead proteins). After incubation the bacterial lysates (adjustment of sample to a total volume of 500 µl) were added to beads and the mixture was again incubated for 30 min at room temperature by usage of end-over-end rotation. Samples were centrifuged (500×*g* for 5 min at 4 °C) and washed three times with 2.5 ml GST binding buffer before elution (300 mM NaCl, 50 mM Tris, 1 mM EDTA, 5 mM EGTA, 5% glycerol, 1 mM DTT, 10 mM reduced glutathione (GSH), pH 7.4) was performed. Therefor, 250 µl elution buffer were added to the resin and after 10 min of incubation at room temperature samples were centrifuged and the supernatant was collected in a new 1.5 ml reaction tube. The step was repeated three times. Afterwards, protein amounts were determined using Bradford reagent and appropriate samples were pooled. Lämmli buffer was added to samples which were used for SDS-analysis. After heating to 95 °C, samples (10 µg each) were applied to an SDS gel. The gel run for 10 min at 150 V and 37 min at 180 V. Because Coomassie staining was not sensitive enough silver staining was done with the ROTI® Black P kit (Carl Roth®) under modified instructions after Blum et al. [21] without formaldehyde. Therefore, the gel was incubated for 1 h in a fixation solution (40% ethanol, 10% acetic acid). After each two washing steps with 30% ethanol and then with water for 20 min, the gel was incubated for 1 min in a 0.02% sodium thiosulfate ($Na_2S_2SO_3$) solution. The gel was washed again with water before incubation at 4 °C with a cold silver nitrate ($AgNO_3$) solution followed. The development step with a 3% sodium carbonate solution containing 0.05% Formalin was done after extensive wash with water. To stop the process and for storage the gel was given into a 5% acetic acid solution. Specific gel bands were cut out and subjected to mass spectrometry.

2.2. Mass spectrometry (MS) analysis of GST-AamA pulldown

Gel bands were prepared for mass spectrometry using the protocol of Shevchenko et al. [22]. The resulting tryptic peptides were desalted using 200 µl StageTips packed with two Empore™ SPE Disks C18 (3 m Purification, Inc., Lexington, KY) according to Ishihama et al. [23] and concentrated using a vacuum concentrator. Samples were resuspended in 15 µl 0.1% formic acid (FA). Peptides were analyzed on an EASY-nanoLC 1200 (Thermo Fisher Scientific, Bremen, Germany) coupled online to a Q Exactive™ Plus mass spectrometer (Thermo Fisher Scientific, Bremen, Germany). 5 µL peptide solution was separated on a 200 cm µPAC™ column (PharmaFluidics, Ghent, Belgium) using a stepped 30 min gradient of 80% acetonitrile (solvent B) in 0.1% formic acid (solvent A) at 700 nL/min flow rate: 4–43% B in 20 min, 43–80% B in 5 min and 80% B in 5 min. Column temperature was kept at 50 °C using a butterfly heater (Phoenix S&T, Chester, PA, USA). The Q Exactive™ Plus was operated in a data-dependent manner in the *m/z* range of 300–1650 with a resolution of 70,000 using an automatic gain control (AGC) target value of 5×10^5 with a maximum injection time of 50 ms. Up to the 12 most intense 2+ - 6+ charged ions were selected for higher-energy c-trap dissociation (HCD) with a normalized collision energy (NCE) of 25%. Fragment spectra were recorded at an isolation width of 1.5 Th and a resolution of 17,500@200 m/z using an AGC target value of 1×10^5 with a maximum injection time of 110 ms. The minimum MS^2 target value was set to 1×10^4. Once fragmented, peaks were dynamically excluded from precursor selection for 10 s within a 10 ppm window. Peptides were ionized using electrospray with a stainless-steel emitter, I.D. 30 µm, (Proxeon, Odense, Denmark) at a spray voltage of 2.1 kV and a heated capillary temperature of 275 °C. The mass spectra were analyzed using MaxQuant (Version 1.6.1.0). At first, parent ion masses were recalibrated using the 'software lock mass' option before the MS^2 spectra were searched using the Andromeda algorithm against protein sequences of *Escherichia coli* strain B-BL21 (Uniprot proteome UP000502174), *Acinetobacter baumannii* 29D2 (GenBank GCA 001693195.1) and the sequence of the recombinant fusion protein GST-AamA. Spectra were searched with a tolerance of 4.5 ppm in MS^1 and 20 ppm in HCD MS^2 mode, strict trypsin specificity (KR not P) and allowing up to two missed cleavage sites. Cysteine carbamidomethylation was set as a fixed modification and methionine oxidation as well as N-terminal acetylation of proteins as variable modifications. The false discovery rate was set to 1% for peptide and protein identifications.

2.3. Construction of plasmids for recombinant production of AcnB and NrdR

Amplification of the *acnB/nrdR* gene of *A. baumannii* strain ATCC® 17978™ was done by PCR using the oligonucleotides *Aconitase-for-pET-24 a (+)*: 5′-ATTACATATGCTAGAAGCTTACCGCCAACACGTTG-3′ (NdeI restriction site underlined) and *Aconitase-rev-pET-24 a (+)*: 5′-ATTACTCGAGAGTCAACTGAGCAGCAGCAATTTTCTTAG-3′ (XhoI restriction site underlined), *NrdR-for-pET-24 a (+)*: 5′-ATTACATATGCATTGTCCATTTTGCAACGCCG-3′ (NdeI restriction site underlined) and *NrdR-rev-pET-24 a (+)*: 5′-ATTACTCGAGGTGCTCACGTTGTTGCATTTGCTC-3′ (XhoI restriction site underlined), respectively. After digestion of pET-24 a (+) expression vector (Novagen) and of amplified genes with restriction enzymes XhoI and NdeI, fragments were ligated. pET-24a(+) carries a kanamycin resistance (Kan^R) cassette, encodes a T7 promotor and is inducible with isopropyl β-D-1-thiogalactopyranoside (IPTG). For protein overproduction the plasmid was transformed into *E. coli* strain BL21 (DE3) pLysS.

2.4. Protein production and purification

In Luria-Bertani (LB)-medium (10 g/L tryptone, 5 g/L yeast extract, 5 g/L NaCl, pH 7.4, 100 µg/ml kanamycin), a 3 ml overnight culture of *E. coli* BL21 (DE3) pLysS pET-24a(+)_*aconitate hydratase 2* or *E. coli* BL21 (DE3) pLysS pET-24a(+)_*nrdR* was grown at 37 °C and 160 rpm. The overnight culture was diluted 1:100 in 200 ml fresh LB-medium (supplemented with 100 µg/ml kanamycin) and was grown in a 2 L bottle-flask at 27 °C for 5 h and 160 rpm. To induce the protein expression, 1 mM IPTG was supplemented and the culture was incubated for another 16 h at 27 °C and 160 rpm. To harvest the cells, cultures were centrifuged (10,000×*g* for 20 min and 4 °C) and pellets were frozen at −80 °C. The pellets were resuspended in 20 ml of cell disruption (CD)-buffer 2 (500 mM NaCl, 50 mM NaH_2PO_4, 20 mM imidazole, 1 mM 1,4-dithiothreitol (DTT), pH 8.0) and the cells were lysed with an Emulsiflex (Avestin). To separate the cell debris from the soluble supernatant, the suspension was centrifuged twice (16,000×*g* for 25 min and 4 °C). For affinity chromatography a His Trap™ High Performance column (5 ml bed volume) which was prepacked with Nickel Sepharose™ High performance was used. The column was equilibrated with 5 column volumes (CV) of binding buffer (composition see CD-Buffer) before the lysate was loaded at a flow rate of 0.5 ml/min. Afterwards, the column was washed with 10 CV of binding buffer. To replace the protein from the column, 8 CV of elution buffer (500 mM NaCl, 50 mM NaH_2PO_4, 500 mM imidazole, 1 mM DTT, pH 8.0) were added performing a linear imidazole gradient. To determine the protein content of the eluted fractions, Bradford reagent (Bio-Rad) was used, and selected fractions were pooled. During all purification steps, 20 µl samples were taken for a later SDS analysis and stored at −20 °C (except samples containing imidazole which were stored at 4 °C).

2.5. Buffer change with PD-10 column

To remove imidazole from samples, a PD-10 column (GE Healthcare Life Sciences) was used. Equilibration of the column was carried out with the PD-10 buffer (150 mM NaCl, 10 mM Tris, 5% Glycerol, 1 mM DTT, pH 7.4) and following steps were done according to the gravity protocol of the manufacturer. Protein concentrations of fractions were again analyzed with the Bradford assay. Pooled fractions were stored at 4 °C before size exclusion chromatography.

2.6. Size exclusion chromatography with HiLoad™ Superdex™ 26/600 200 pg

AcnB appeared as a mixture of different oligomers (monomer, dimer and aggregate). To resolve the oligomers, after buffer change the sample (6 ml) was applied to a HiLoad™ Superdex™ 26/600 200 pg (prep grade) column (bed volume 320 ml). The column was equilibrated with 1 1/2 CV of Superdex buffer (20 mM Tris-HCl, 100 mM NaCl, 3% glycerol, 1 mM DTT, pH 8.0). After the pooled fraction was applied, the column was washed with 220 ml buffer before all oligomeric states of the AcnB were fully fractionated. Protein concentrations of all samples were determined with the Bradford assay and subsequently pooled depending on their oligomeric state. For a higher concentration of monomer, dimer, and aggregate fractions, samples were concentrated via a Vivaspin® 20 ultrafiltration unit (30.000 MWCO, PES-Polyethersulfone, Sartorius AG) and were used immediately or stored at −80 °C.

3. Investigation of interactions between AcnB and AamA

3.1. Co-immunoprecipitation

Co-immunoprecipitation was applied to study interactions between AcnB and AamA. 3 μl AcnB (4.9 mg/ml) and 7.5 μl AamA (2 mg/ml) or BSA (2 mg/ml) as a control each were again incubated alone or together for 15 min at 4 °C. Then 2 μl of the 6x His tag monoclonal primary antibody (his.h8) (conc. 1 mg/ml, Invitrogen) was added to the samples and the mixture was incubated for 1 h at 4 °C on a table shaker (controls did not include the primary antibody). Then 20 μl A/G PLUS Agarose (Santa Cruz® Biotechnology) was added, and samples were adjusted to 100 μl with the same buffers used for buffer change and size exclusion chromatography. After incubation for 1 h at 4 °C on a table shaker, samples were centrifuged at 580×*g* for 5 min at 4 °C and agarose beads were washed 4 times with buffer used for buffer change and size exclusion chromatography. Then bead pellets were resuspended in 40 μl electrophoresis sample buffer (modified after Lämmli: 0.1% 2-Mercaptoethanol, 2.5 mM Tris pH 8.8, 0.05% glycine, 0.35 mM SDS, 1 mM magnesium chloride ($MgCl_2$), 0.001% Bromphenol blue) and after heating for 5 min at 95 °C, the samples were applied on a sodium dodecyl sulfate (SDS)-gel. The gel was running in a mini-PROTEAN® 3 cell chamber (Bio-Rad) for 10 min at 150 V and for 37 min at 180 V. For detection of protein bands, the gel was stained with Coomassie brilliant blue (25% isopropyl alcohol, 10% acetic acid, 0.05% Coomassie brilliant blue R-250, 65% Aqua dest.) and after 1 h the gel was de-stained (50% methanol, 7% acetic acid, 43% Aqua dest) for 45 min.

3.2. Production of pre-adsorbed anti-AamA antiserum

For pre-adsorption of the A1S_0222 antibody (rabbit antiserum raised against GST-AamA with 4 injections of 150 μg each following standard protocols: Dr. Pineda, Berlin, Germany) an overnight culture (50 ml) of *E. coli* strain BL21 and *A. baumannii* mutant strain 202/4 was grown. Next, the cultures were centrifuged, and the pellets from 25 ml of culture each were resuspended in 3 ml PBS (phosphate buffered saline). Afterwards, cells were lysed via ultrasonication. Then the solutions were again centrifuged twice, and 3 ml of each supernatant were mixed with 1.5 ml of rabbit serum and were incubated for 60 min on ice under constant panning. Samples were frozen at −20 °C and tested by Western blotting.

3.3. Western blots

The Bis-Tris gels (BN-PAGE) as well as the SDS-gels were made in duplicate to transfer the protein bands on a nitrocellulose membrane for a subsequent immuno-detection in parallel to the Coomassie stained gels. For blotting, the anode-buffer 1 (300 mM Tris pH 8.8, 20% methanol), anode-buffer 2 (25 mM Tris pH 8.8) and cathode-buffer (25 mM Tris pH 8.8, 40 mM aminocaproic acid, 0.01% SDS) were used to soak the blot paper (Bio-Rad). The blot was run for 18 min at 22 V and 150 mA. Afterwards, the membrane was first incubated in blocking solution (25 mM Tris pH 8.8, 0.5% Tween 20, 1% milk powder, 1% BSA, pH 7.5) for 1 h at room temperature and then the pre-adsorbed primary antibody α-AamA (diluted 1:5000 in blocking solution) was given to the membrane and was again incubated over night at 4 °C. Next, the membrane was washed 3 times for 5 min with PBS plus 0.5% Tween 20. After washing, the secondary antibody α-rabbit horseradish peroxidase (HRP-diluted 1:5000 in blocking solution) was given to the membrane for 1 h at room temperature and then the membrane was again washed 3 times for 5 min before the blot was developed with 3,3′-diaminobenzidine tetrahydrochloride (DAB-SIGMA). Therefor, 30 μl of the DAB chromagen solution were added to 1 ml of the DAB buffer solution and after well mixing the membrane was incubated with until red/brown signals were detectable. Afterwards, the solution was discarded, and the membrane was washed with aqua bidest for 5–10 min and dried under exclusion of light.

3.4. Construction of plasmid for recombinant production of pyrimidine deaminase RibD (A1S_0221)

For production of RibD the pGEX-6P-3 plasmid was used. Amplification of *ribD* (A1S_0221) of *Acinetobacter baumannii* ATCC 17978 was done by PCR using the oligonucleotides *Deaminase-for-pGEX-6P-3*: 5′-ATTAGGATCCTCTGAGTTAAAACAAGATCAATACTGGATGCAGC-3' (*Bam*HI restriction site underlined) and *Deaminase-rev-pGEX-6P-3*: 5′-ATTAGCGGCCGCTCATACTTTCTCTTGCGTAGGG-3′ (*Not*I restriction site underlined). After digestion of the pGEX-6P-3 expression vector (Novagen) and the amplified *ribD* with restriction enzymes *Bam*HI and *Not*I, the fragment was cloned into the vector. pGEX-6P-3 carries an ampicillin resistance (Amp^R) cassette, possesses an IPTG-inducible *tac* promotor, and encodes a PreScission protease cleavage site. For protein expression, the plasmid was transformed into *E. coli* strain BL21 (DE3) pLysS.

3.5. RibD production and purification

In LB medium supplemented with 100 μg/ml ampicillin, a 3 ml overnight culture of *E. coli* BL21 (DE3) pLysS pET-24 a (+) *_A1S_0221* was grown at 37 °C and 160 rpm. The overnight culture was diluted 1:100 in 200 ml fresh LB medium (supplemented with 100 μg/ml Amp) and was grown in a 2 L bottle-flask at 27 °C for 5 h and 160 rpm. To induce the protein expression, 0.5 mM IPTG was supplemented and the culture was incubated for another 16 h at 27 °C and 160 rpm. To harvest the cells, cultures were centrifuged (10,000×*g* for 20 min and 4 °C) and pellets were frozen at −80 °C. The pellets were resuspended in 20 ml of cell disruption (CD)-Buffer 3 (300 mM NaCl, 5 mM EGTA (ethylene glycol-bis(2-aminoethylether)-N, N, N', N'-tetra-acetic acid), 1 mM EDTA (2, 2′, 2″, 2‴-(ethane-1,2-diyldinitrilo)-tetra-acetic acid), 1 mM DTT, 5% glycerol, 2 U Benzonase nuclease (250 U/μl), pH 7.4) and the cells were lysed with an Emulsiflex (Avestin). To separate the cell debris from the soluble supernatant, the suspension was centrifuged twice (16,000×*g* for 25 min and 4 °C). For affinity chromatography a GSTPrep™FF 16/10 column (20 ml bed volume) was used according to the manufacturer's instructions. First the column was equilibrated with 5 column volumes (CV) of Binding buffer (300 mM NaCl, 1 mM EDTA, 5 mM EGTA, 5% glycerol, 1 mM DTT, pH 7.4) before the lysate was loaded at a flow rate of 0.5 ml/min. Afterwards, the column was washed with 5 CV of Binding buffer. To replace the protein from the column, 6 CV of Elution buffer (1000 mM NaCl, 50 mM Tris, 1 mM EDTA, 10 mM reduced glutathione (GSH), 5% glycerol, 1 mM DTT, pH 7.4) were added. To determine the protein content of the eluted fractions, Bradford reagent (Bio-Rad) was used, and appropriate fractions were pooled. For all purification steps, 20 μl samples were taken for later SDS-PAGE

analysis and stored at −20 °C. To cut off the GST-Tag, the pooled sample with a protein amount of 14 mg was incubated for 16 h at 5 °C with 60 U of PreScission protease.

3.6. Buffer change with a HiPrep™ 26/10 column and removal of the GST-tag

To remove GSH, the pooled protein sample after incubation with the PreScission protease and subsequent centrifugation (10,000×*g* for 20 min and 4 °C) was applied to the HiPrep™ 26/10 desalting column. Preparation of the column was according to the manufacturer's instructions. The column was equilibrated with 3 CV B1 buffer (150 mM NaCl, 10 mM Tris, 5% Glycerol, 1 mM DTT, pH 7.4), before the sample was loaded at a flow rate of 0.5 ml/min. Afterwards the column was washed with B1 buffer and the flow-through was collected in 1 ml fractions. Protein quantity determination of fractions was again carried out with the Bradford method. Removal of cleaved GST-tag, un-cleaved fusion protein and GST-tagged PreScission protease from pooled fractions was then achieved during a second purification step using a GSTPrep™FF 16/10 column (20 ml bed volume) equilibrated with B1 buffer. The sample was applied at a low flow rate (0.3 ml/min) to bind GST protein. Pooled flow-through fraction was concentrated with a Vivaspin® 15R ultrafiltration unit (10.000 MWCO, HY-Hydrosart®, Sartorius AG). The protein was stored at −80 °C until further analyses.

4. Investigation of interactions between RibD, NrdR and AamA

4.1. Blue native-polyacrylamide gel electrophoresis (BN-PAGE)

To investigate possible interactions between AcnB, NrdR or RibD with AamA, Blue native-PAGE (BN-PAGE) was performed. First, the respective proteins and AamA were incubated at final concentrations indicated in the respective figure legends for 15 min at 4 °C. Bovine serum albumin (BSA, final conc. 2 μg/μl) was used as a control (in assays with AcnB and NrdR). After incubation, NativePAGE™ 5% G-250 sample additive (0.25–1 μl or $\frac{1}{4}$ of detergent concentration) and NativePAGE™ sample buffer (4x) was added to samples composed of single protein or protein mixtures and were then applied to a NativePAGE™ Novex® 4–16% Bis-Tris gel (10 well). Electrophoresis was performed in a XCell™ *SureLock*™ Mini-Cell (Life Technologies™) filled with anode buffer (NativePAGE™ running buffer (20x): 50 ml, deionized water: 950 ml) in the outer buffer chamber and cathode buffer (Dark blue: NativePAGE™ running buffer (20x): 10 ml, NativePAGE™ cathode additive (20x): 10 ml, deionized water: 180 ml) in the inner buffer chamber, for 120 min at 150 V (constant).

4.2. Electrophoretic mobility shift assay (EMSA)

EMSA was applied to study interactions between AamA and amplified DNA fragments. To this end, each DNA fragment was pre-incubated alone or together as a mixture with AamA for 30 min at room temperature. To see if S-adenosylmethionine (SAM) has an influence on AamA-DNA interactions, SAM was added to selected samples. After incubation, samples were mixed with 3 μl 10x buffer (0.25% Bromophenol Blue, 30% Glycerin in TAE buffer) and afterwards applied to a 6% bis-acrylamide gel (40% acrylamide:bisacrylamide, 5x TBE (TRIS-Borate-EDTA) buffer, 10% freshly prepared APS (ammonium peroxodisulfate), TEMED (N, N, N', N'-tetra-methyl-ethylene-diamine), adjustment with aqua bidest [24]). The gel was pre-run in 0.5x TBE buffer (pH 8.0) for 20 min at 80 V and for another 120 min after application of samples. The electrophoresis chamber was kept on ice the whole time. Gels were stained using a silver staining kit (ROTI®Black P silver staining kit, Carl Roth) following manufacturer's instructions. Next to the bis-acrylamide gel, samples were also applied to an agarose gel using 1.5% Roti® garose in 0.5 x TBE (Tris-Borate-EDTA, pH 7.0) buffer. For later visualization of DNA fragments, the staining dye GelRed® (1:10000, Biotium) was added to the still liquid agarose solution. After samples were applied to the gel, electrophoresis was run for 45 min at 150 V and 400 mA before detection with UV light using a Geldoc (Bio-Rad). The GST gene (including promotor region) as a control was amplified using oligonucleotides *Glutathione-S-Transferase-for*: 5′-GACATTCATACTGTGCTTGT TACAGC-3′ and *Glutathione-S-Transferase-rev*: 5′-CTTTTATATATCAGC ACAATTTCTTTCGTTTGACCG-3′. The Rrf2 gene (including promotor region) harbouring one AamA-specific methylation site was amplified using oligonucleotides *Rrf2-for*: 5′-GGTGGCGTTCGTAAGTTTTCC-3′ and *Rrf2-rev*: 5′-CGGCTTATTAGCTCATTAGTCGGGAG-3′.

4.3. Reverse Transcriptase polymerase chain reaction (RT-PCR)

In *A. baumannii* strain ATCC 17978, *aamA* (A1S_0222) is flanked by *nrdR* (A1S_0220), *ribD* (A1S_0221), and *ribE (*A1S_0223). To examine expression of each single gene and putative polycistronic transcripts (A1S_0220-A1S_0223), RNA from strain 29D2 was extracted using the RNeasy mini kit (Qiagen) following manufacturer's instructions. 1 μl RNA (175 ng/μl) was transcribed into cDNA using the RevertAid First Strand cDNA Synthesis Kit (Thermo Fisher Scientific) following manufacturer's instructions. For reverse transcription of RNA into cDNA 4 μl specific primers (reverse primers, 20 pmol: *RibD-RT-rev*: 5′-GGATCCGGCGCTTGTTACCCAAATAC-3′, *AamA-rev*: 5′-GGATCCGTGA-GACAGATCCCGTTAGTTGC-3′, *RibE-rev*: ATTAGGATCCTTGGGTCGG-CACACACTCAG-3′) for individual gene segments each were used. After addition of 7 μl aqua bidest, samples were incubated for 5 min at 65 °C. Then, samples were carefully mixed and 4 μl 5x reaction buffer, 1 μl RiboLock RNase inhibitor (20U/μl), 2 μl 10 mM dNTP mix and 1 μl RevertAid M-MuLV Reverse Transcriptase (200 U/μl) were added. After briefly centrifugation the mixture was incubated for 1 h at 42 °C. To stop the reaction, samples were incubated for 5 min at 70 °C. In a subsequent PCR, genomic DNA, RNA or cDNA was used as template together with specific primers (A1S_0222: *AamA-for*: 5′-GGATCCGGATGAAATGAT-CAGTTATGTGGC-3′and *AamA-rev*: 5′-GGATCCGTGAGACAGATCCC GTTAGTTGC-3′; A1S_0221: *RibD-for*: 5′-GGATCCTATTTGCACTTGACC ACGTTGCC-3′and *RibD-RT-rev*: 5′-GGATCCGGCGCTTGTTACCCAAA-TAC-3′; A1S_0221-A1S_0222: *RibD-for*: 5′-GGATCCTATTTGCACTT-GACCACGTTGCC-3′ and *AamA-rev*: 5′-GGATCCGTGAGACAGATCCCG TTAGTTGC-3′; A1S_0220-A1S_0223: 5′-GGATCCGTCTTGTGCTGTGAT-CAAAGCG-3′ and *RibE-rev*: ATTAGGATCCTTGGGTCGGCACA-CACTCAG-3′; for a more descriptive representation see **S. 6**).

4.4. Chemical crosslinking

The physical proximity of interacting proteins can lead to the formation of covalent bonds in the presence of chemical crosslinkers. Amine-reactive NHS ester (N-hydroxysuccinimide esters) of used cross linkers Sulfo-EGS (ethylene glycol bis(sulfosuccinimidyl succinate)), EGS (ethylene glycol bis(sulfosuccinimidyl succinate)) and DSP (dithiobis(succinimidyl propionate; Lomant's Reagent)) can form covalent amid bounds with primary amines of protein side chains. Because of the primary amine nature of Tris, all used protein samples were rebuffered to cross linking buffer (10-fold diluted PBS supplemented with 150 mM NaCl, 5% Glycerol, pH 7.4) before. Afterwards, AamA (10 μM) was incubated with RibD (10 μM) or AcnB (10 μM) and cross linker (5 mM) for 30 min at room temperature (total volume: 50 μl). Reaction was stopped applying Lämmli buffer. After 15 min of incubation, samples were applied on an SDS-gel that was stained or Western-blotted.

4.5. Small-angle X-ray scattering (SAXS)-Implementation

Small angle X-ray scattering (SAXS) data $I(s)$ vs. s nm^{-1} ($s = 4\pi\sin\theta/\lambda$; 2θ is the scattering angle and λ the X-ray wavelength, 0.124 nm) were measured at the EMBL-P12 bioSAXS beam line (DESY, Hamburg [25]). The protein samples and corresponding matched solvent blanks were measured

at 20 °C using standard batch mode sample delivery with an automated sample changer robot. The sample conditions were: i) Riboflavin biosynthesis protein, RibD (1.6 mg/ml) in 150 mM NaCl, 10 mM Tris, 1 mM DTT, 5% v/v glycerol, pH 7.4, and; ii) Aconitate hydratase B, AcnB (4.7–4.9 mg/mL) or the transcriptional repressor NrdR (1.4 mg/ml) in 100 mM NaCl, 20 mM Tris, 1 mM DTT, 3% v/v glycerol, pH 8.0. The SAXS data were recorded in sets of 0.1 s individual data frames recorded on a 2D Pilatus 6 M detector for a total X-ray exposure time of 6–8 s. All post processing data routines including data reduction via 2D-to-1D azimuthal averaging, the automated rejection of data-frames affected by radiation damage, final individual data-frame averaging and background subtraction, were performed using the *SASFLOW* pipeline [26]. The resulting 1D-reduced and background-subtracted SAXS data were normalized to sample transmission and concentration and placed on an absolute scale ($I(s)$, cm^{-1}) relative to the scattering from water. The data were also compared to the scattering measured from a bovine serum albumin standard (BSA, at 2.38 mg/ml in 50 mM HEPES, pH 7.4) using identical measurement and instrument parameters.

4.6. Small-angle X-ray scattering (SAXS)-Analyses

The SAXS data underwent analysis to extract structural parameter information, including concentration-dependent and concentration-independent molecular weight (MW) estimates; the Porod volume (V_p), radius of gyration (R_g) and maximum particle dimensions (D_{max}) using a combination of standard procedures (Guinier approximation (ln ($I(s)$ vs s^2) [27], Kratky plots ($I(s)s^2$ vs s) and the indirect inverse Fourier transform of the data, i.e., the calculated probable real-space pair--distance distribution functions, or $p(r)$ profiles [28]. *Ab initio* bead modelling, or dummy residue (DR) modelling was performed – when relevant – using *DAMMIN* [29] or *GASBOR* [30], respectively, while any pertinent mixture DR-modelling analysis (specific to AcnB) was performed using *GASBORMX* [31]. Additional atomistic representations of either RibD or AcnB were developed using homology models derived from the X-ray crystal structure of a closely related RibD isoform (Protein databank, PDB: 3ZPG [7]), or the predicted Alphafold2 [32] model of AcnB, that were used as templates for rigid-body modelling. An iron-sulfur cluster (3Fe–4S) was added to the active site of AcnB based on the structural alignment of the AlphaFold2 homology model to the X-ray crystal structure of the *Escherichia coli* isoform (PDB 1L5J [33]). The spatial positioning of the domains within the RibD or AcnB proteins to satisfy fits to the SAXS data were performed using *SASREF* [34] while the normal mode analysis of possible RibD domain movements were performed using *SREFLEX* [35]. In all instances, the quality of the model fits to the SAXS data were assessed using *CRYSOL* (implicit hydration shell [36]), or *CRYSOL3* (explicit hydration shell [37]) and evaluated according to the reduced χ^2 test or Correlation Map (CorMap) p-value [38]. The fitting parameters were: 30 spherical harmonics, with 256 points to a s_{max} between 3.0 and 3.5 nm^{-1} with or without a constant adjustment. The SAXS data and any relevant models have been deposited to the Small Angle Scattering Biological Data Bank (SASBDB [39] under the accession codes: RibD SASDNC5; AcnB, SASDND5 and SASDNE5; NrdR SASDNF5.

5. Results

5.1. Overproduction and purification of AcnB

In an attempt to identify possible interaction partners of AamA, a pulldown assay using GST-AamA as bait was performed with bacterial lysates of *A. baumannii* wildtype strain 29D2 and the associated *aamA*$^-$ mutant as a control, followed by silver-stained SDS gel analysis and mass spectrometry (S. 7, Supplementary Table 2). Aconitate hydratase (AcnB) was identified as a potential partner of AamA with highest MALDI-TOF score. AcnB represents a key enzyme of the citrate cycle making it ideally suited to coordinate cell physiology and epigenetic regulatory activity of AamA. AcnB was cloned as a fusion protein with a C-terminal His-tag and thus purified using a HisTrap™ High Performance column. The NaCl concentration in pooled fractions was subsequently reduced from 500 mM to 100 mM and the imidazole removed applying a PD-10 column. Since we observed aggregation of AcnB applying small-angle X-ray scattering (data not shown), we applied size exclusion chromatography to characterize the desalted fractions on a HiLoad® 26/600 Superdex column. We observed three peaks representing monomers, dimers and aggregates of AcnB as estimated from the calibration of the column. In the absence of the reducing agent DTT, the portion of the aggregates was higher in comparison to that of the monomers and dimers. With DTT, the aconitase monomer and dimer fractions increased (Fig. 1). Monomer and dimer fractions were successfully concentrated on polyethersulfone ultracentrifugation devices while concentration of aconitase aggregates failed. Purification of the aconitase (95 kDa) is shown in Fig. 2 and summarized in Table 1 The yield is 7.27 mg of monomer and 6.61 mg of dimer from 200 ml of culture. The monomeric fraction as well as the dimeric fraction of AcnB proved to be active in an enzymatic assay detecting the consumption of aconitate which points out the correct folding of AcnB.

5.2. Structural analysis of AcnB via small angle X ray scattering (SAXS)

The *A. baumannii* AcnB isoform (UniProt V5VBJ4) shares 74% sequence identity to the *E. coli* homologue (UniProt P36683), and the resulting AlphaFold2 predicted model of the *Acinetobacter* protein appears structurally similar to the previously determined X-ray crystal structure of *E. coli* AcnB (PDB 1L5J; Chain A, RMSD Cα = 0.4 Å). The protein is characterized as having a three-domain architecture consisting of a N-terminal HEAT-repeat domain (amino acids ~ 1–157), a middle 'cap' domain (amino acids ~ 165–364), and a C-terminal 'cup' domain (amino acids ~ 386–879) that also contains an active site iron-sulfur cluster. The linker between the N-terminal HEAT-repeat and middle-cap domains is approximately 6–7 amino acids, while the linker connecting the middle-cap and the C-terminal cup domains is particularly long at 22–23 amino acids. In both the X-ray crystal structure of the *E. coli* AcnB homologue and the predicted AlphaFold2 AcnB model, the three domains pack close together. The middle-cap and C-terminal cup domains form an interface that generates the aconitate binding and enzyme active site. In effect, the cap domain covers the cup domain. The HEAT-repeat generates a funnel-like structure proximal to, and with, the middle-cup domain forming a tunnel down toward the Fe–S cluster of the active site. The *E. coli* homologue crystallizes with a symmetry related protomer to form a dimeric biological assembly.

The aconitate hydratase SAXS data and models are presented in Fig. 3, and the SAXS-based structural parameters in Supplementary Table 3. The interpretation of the SAXS results suggest that *A. baumannii* AcnB is a structurally diverse protein that synergizes intramolecular domain movements and intermolecular association states in solution. Two AcnB samples were isolated for the SAXS measurements: i) a monomeric fraction based on gel filtration and native PAGE analyses and, ii) a second fraction designated as dimeric. The analysis of the structural parameters obtained from the SAXS data, in particular the MW and Porod volume estimates, indicate that the suspected monomeric fraction is actually monomeric (MW = 92–103 kDa, V_p = 150 nm^3; expected MW, monomer = 96 kDa), while the dimeric fraction, even at the relatively high concentration of 4.7 mg/ml, presents as a mixture of monomers and dimers (MW = 127–162 kDa, V_p = 230 nm^3; expected MW, dimer = 192 kDa). For the monomeric AcnB, the R_g and D_{max} determined from the SAXS data are 3.5 and 12.5 nm, respectively, which are larger than the R_g and D_{max} calculated from the *E. coli* monomer structure or Alphafold predicted models (R_g = 3.1 nm; D_{max} = 9.6 nm). The increase in R_g of 0.4 nm, and a D_{max} of almost 3 nm, indicates that a redistribution in mass has occurred within the monomeric form of the protein relative to the overall compact domain arrangement observed in the *E. coli* AcnB homologue or Alphafold models. Indeed, both of these

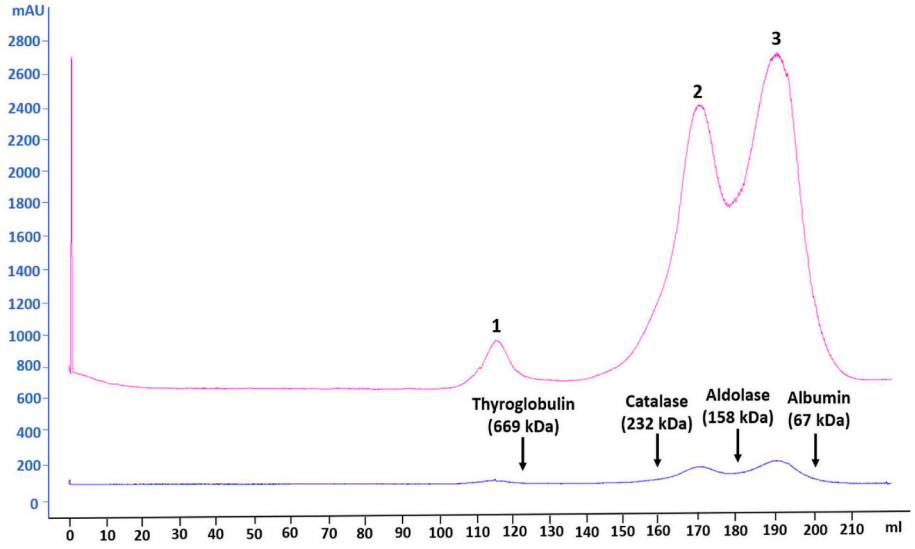

Fig. 1. Chromatogram of Aconitate Hydratase 2 (AcnB) gel filtration on HiLoad™ 26/600 Superdex™ 200 pg:
The absorption in mAU (milli Absorption Unit) is plotted on the y-axis, and the x-axis shows the volume in ml passed through the system. The absorption spectrum is shown at 280 nm (blue curve) and at 215 nm (magenta curve). Numbers point out oligomerization states of AcnB (1: Aggregate, 2: Dimer, 3: Monomer); column calibration with protein standards is indicated.

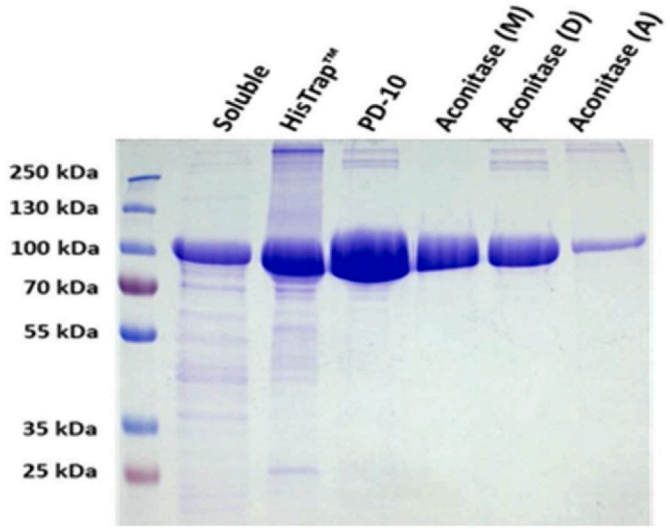

Fig. 2. Purification of Aconitate Hydratase 2 (AcnB):
Sodium-dodecyl-sulfate (SDS) gel representing single steps of AcnB purification, including supernatant after centrifugation of cell-debris (soluble), AcnB after HisTrap™ HP (5 ml, Ni-Sepharose) column, AcnB after buffer change via PD-10 Column, concentration of AcnB oligomerization states (M: Monomer, D: Dimer and A: Aggregate) using a Vivaspin® ultrafiltration unit with a Hydrosart® membrane.

initial AcnB structures do not fit the SAXS data with χ^2 in excess of 200 (CorMap $p = 0$). However, if the N-terminal-HEAT, middle-cap and C-terminal cup domains are allowed to shift position relative to each other, reasonable atomistic representations maybe obtained that fit the SAXS data (CRYSOL χ^2 range = 1.2–1.6, CorMap $p = 0$–0.004; CRYSOL3 χ^2 range = 1.17–1.25, CorMap $p = 0.004$–0.1). These rigid-body refined models show the alternative spatial sampling of the N-terminal HEAT domain and, in addition, there appears to be a consensus across the model cohort that the middle cap domain spatially shifts away from the C-terminal cup domain, separating the interface and opening the active site cleft. The resulting *ab initio* shape restoration of the monomer using *DAMMIN* bead modelling or *GASBOR* dummy residue modelling, generate shapes that fit the data ($X^2 = 1.0$, CorMap $p = 0.001$–0.1) that are spatially consistent with the more open forms of the monomer. Combined, the solution-state models suggest that the AcnB monomer may have an ability to sample multiple structural states that, on average, adopt a more open domain conformation relative to the more compact *E. coli* AcnB X-ray crystal structure or Alphafold predicted models. Complicating the interpretation of the SAXS data is that the second isolated fraction of AcnB presents as a mixture of monomers and dimers in solution, of approximately 65% and 35% volume fraction, respectively. *GASBORMX* mixture models maybe obtained that fit the monomer-dimer fraction SAXS data considering these volume fractions ($\chi^2 = 1.0$, CorMap $p = 0.03$–0.9). However, attempts at obtaining reasonable rigid-body/atomistic models of the monomer-dimer mixture were unsuccessful. It may be that the association between AcnB monomers triggers an alteration in the spatial sampling of the domains within each protomer of the dimer, making it difficult to describe the AcnB as simple volume-fraction weighted mixture of two structural components. In summary, and based on the SAXS data measured under the described experimental conditions, *A. baumannii* AcnB appears as a structurally diverse protein that combines elements of both conformational sampling. Beside structural analysis of the AcnB protein alone, also mixtures with AamA were studied via SAXS. However, there was no evidence of a potential interaction between AcnB and AamA.

Table 1
Purification table of Aconitate Hydratase 2 (AcnB):
Table showing single steps of AcnB purification. For protein purification a 200 ml *E. coli* culture was used. The weight of the wet pellet was 2 g. Purity was calculated with the ImageJ program.

Purification step	Total Volume [ml]	Protein Conc. [mg/ml]	Total Protein [mg]	Total AcnB [mg]	Purity AcnB [%]	Purification [fold]
Soluble bacterial lysate	38	3.68	139.84	105.57	75.49	1
HisTrap™	6	6.57	39.42	31.14	81.54	1.1
PD-10	5	6.4	32	30.47	95.21	1.26
Vivaspin® 20 PES (M)	1.5	4.9	7.35	7.27	98.93	1.31
Vivaspin® 20 PES (D)	1.5	4.7	7.05	6.61	93.79	1.24
Vivaspin® 20 PES (A)	1.5	0.4	0.6	0.56	93.01	1.23

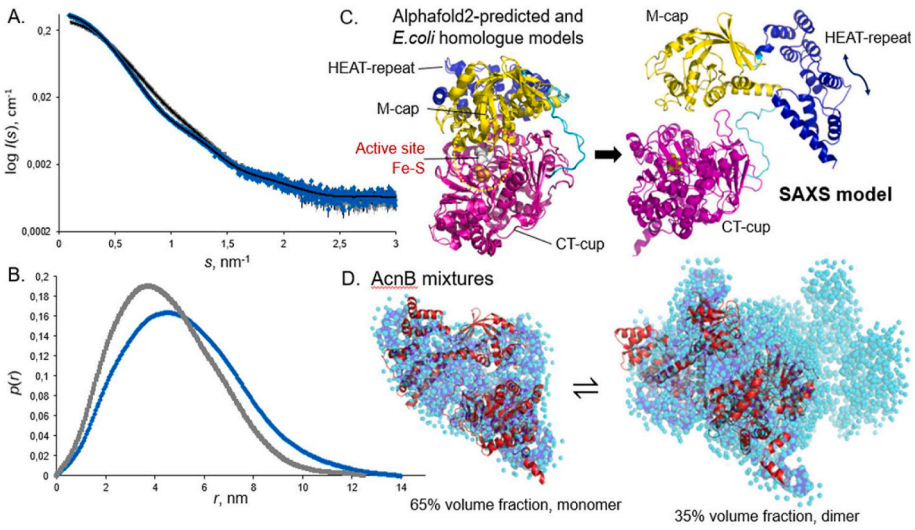

Fig. 3. SAXS data and modelling of AcnB: **A.** AcnB monomer SAXS data (grey squares) and monomer-dimer mixture data (blue diamonds) with a representative model fit example (black lines, refer to panel D). **B.** The corresponding *p(r)* profiles of the real-space distance frequencies. In this case the monomer-dimer *p(r)* profile (blue diamonds) should be interpreted as a volume-fraction weighted distribution of frequencies of the mixtures. **C.** Spatial overlay of the Alphafold2 predicted and the X-ray crystal structure of a closely related *E. coli* homologue (PDB: 1L5J) highlighting the three main domain features of the protein, an N-terminal HEAT repeat (blue ribbons), a middle-'cap'domain (yellow ribbons) and a C-terminal 'cup'domain (magenta ribbons) that are connected by linkers (cyan). In order to fit the monomer-fraction SAXS data, the three domains appear to undergo a spatial rearrangement that opens up the structure ($\chi^2 = 1.2$) relative to the predicted X-ray models ($\chi^2 > 200$, refer to SASBDB entry SASDND5). **D.** *GASBORMX* DR-models (cyan-spheres) and the associated volume-fractions of monomer and dimer obtained after modelling the AcnB monomer-dimer mixture data (monomer $\chi^2 = 1.0$; dimer $\chi^2 = 1.05$, black line panel A). A spatial overlay of the monomer model from panel C is shown as red ribbons. Refer to SASBDB entry SASDNE5.

5.3. Overproduction and purification of NrdR (A1S_0220)

NrdR is a small protein of 18 kDa which is encoded by the *nrdR* gene located upstream of the *aamA* gene in strain ATCC 17978. Proximity of both genes made us speculate of NrdR as another possible interaction partner of AamA. Like AcnB, also NrdR was cloned as a fusion-protein with a C-Terminal His-tag. The protein was purified using a HisTrap™ High Performance column and subsequent buffer change on PD-10 column. Concentration of the NrdR protein with ultrafiltration units wasn't successful although different membrane compositions were tested. Purification of NrdR is shown in Fig. 4 and summarized in Table 2. The yield of NrdR was 5.6 mg although the expression level was high as was solubility in the cleared lysate pointing to a problem of solubility induced by purification. The aberrant migration of NrdR in SDS gels (apparent mass of 15 kDa rather than 18 kDa) might be due to hydrophobicity which would also explain the failure to concentrate NrdR.

5.4. Structural analysis of NrdR via small angle X ray scattering (SAXS)

The putative transcriptional repressor NrdR is a small protein of approximately 18 kDa with an unusual predicted alphafold structure characterized by two short sections of beta sheet connected by a linker at the N-terminus, followed by a compact C-terminal α-helical bundle (https://alphafold.ebi.ac.uk/entry/A3M1A1). The SAXS data measured from NrdR demonstrates that the protein has a strong propensity to self-associate into what appears to be large (<500+ kDa) macromolecular assemblies that have characteristics of a repeat-unit filamentous-like structure (Fig. 5). There is a characteristic 'hump' in the data observed between the *s*-range of 0.58–1 nm^{-1}, with a peak maximum at approximately 0.75 nm^{-1}. This region of the profile maybe interpreted as a weak diffraction peak and corresponds to real space distances internal to the assemblies spanning 6.3–10.8 nm, with a most common modular repeat distance of approximately 8.4 nm that is similar in magnitude to the D_{max} of the predicted NrdR monomer (8.3 nm). The dimensionless Kratky plot representation of the data indicates that the NrdR assemblies form long and extended structures, while the corresponding estimate of the *p*(r) suggests that, in general, the assemblies are long, extended and rod-like (with maximum dimension in excess of 90 nm and an approximated cross section diameter of around 10 nm). When aliquots of DNA-(adenine N6)-methyltransferase (AamA) are added to the NrdR

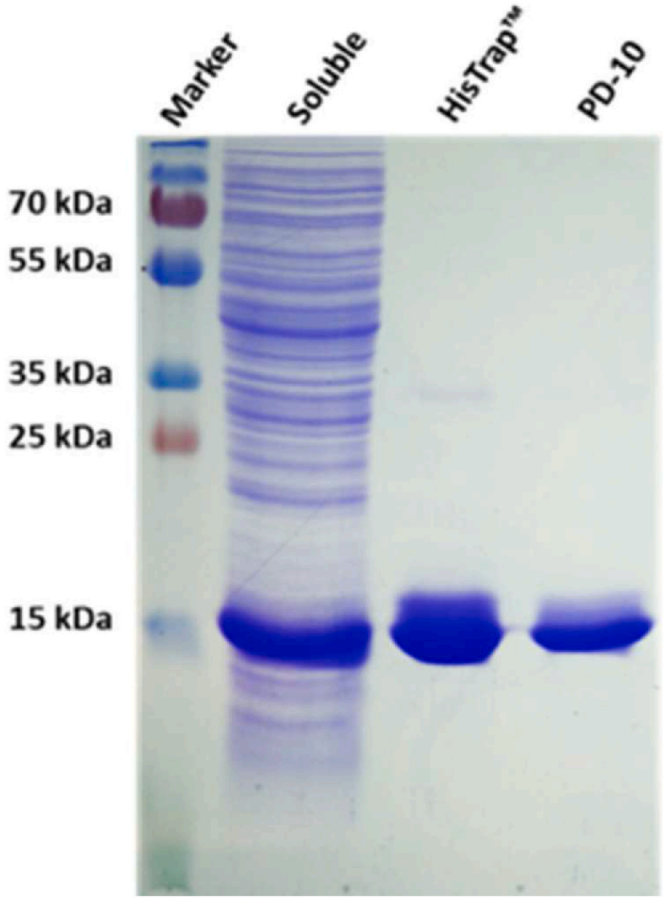

Fig. 4. Purification of putative transcriptional repressor NrdR (A1S_0220): SDS gel representing individual steps of NrdR purification, including supernatant after centrifugation of cell-debris (soluble), NrdR after HisTrap™ HP (5 ml, Ni-Sepharose) column and buffer change using a PD-10 column.

Table 2
Purification table of NrdR (A1S_0220):
Table showing single steps of NrdR purification. For protein purification a 200 ml *E. coli* culture was used. The weight of the wet pellet was 2 g. Purity of NrdR was calculated with the ImageJ program.

Purification step	Total Volume [ml]	Protein Conc. [mg/ml]	Total Protein [mg]	Total NrdR [mg]	Purity NrdR [%]	Purification [fold]
Soluble bacterial lysate	33	4.37	144	86.4	60	1
HisTrap™	5	2.86	14.3	14.3	91.3	1.52
HiPrep™ 26/10	4	1.4	5.6	5.6	99.4	1.65

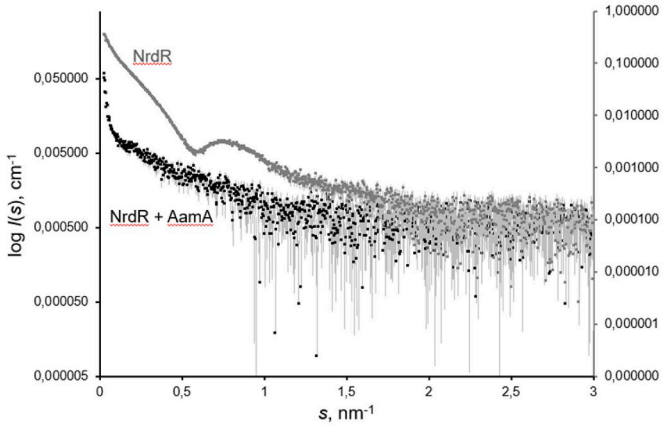

Fig. 5. SAXS data of NrdR:
A comparison between the SAXS data measured for large filamentous-like assemblies of NrdR (A-grey squares) compared to a mixture of NrdR and AamA (B-black squares) showing the significant reduction in scattering intensity as AamA disrupts the NrdR assemblies.

assemblies, a radical alteration in the SAXS profiles are observed. The AamA appears to disassemble the NrdR filaments into a likely polydisperse system of much smaller particles and non-specific aggregates, as evidenced in a significant decrease in the scattering intensities. The results are presented in Fig. 5.

5.5. Overproduction and purification of pyrimidine deaminase/reductase RibD (A1S_0221)

Between *nrdR* and *aamA* in *A. baumannii* strain ATCC 17978, another gene, A1S_0221, is located which encodes a pyrimidine deaminase/reductase (*ribD*) that we considered as an additional potential interaction partner of AamA. The protein was cloned as a fusion-protein with an N-terminal GST-tag. The lysate was applied to a GSTPrep™FF 16/10 column for affinity chromatography. After elution with glutathione (GSH), the GST-Tag could be cleaved off completely using PreScission protease. GSH was subsequently removed using a HiPrep™ 26/10 desalting column. Removal of the detached GST-Tag, of GST-tagged PreScission protease and GST-RibD residual was achieved by a second affinity chromatography step using a GSTPrep™FF 16/10 column again. The pyrimidine deaminase could be concentrated via a HY-Hydrosart 15R ultrafiltration unit (10.000 MWCO) (Table 3). Purification of the pyrimidine deaminase (42 kDa) is shown in Fig. 6 and summarized in Table 3. The yield of RibD was 2.79 mg from a 200 ml culture with an approximately 2 g wet pellet. In comparison to NrdR and AcnB, the total protein amount in the soluble lysate of RibD is much lower. One explanation could be the different expression vector (pGEX-6P-3 instead of pET-24 a(+)). Moreover, RibD purification was performed using the purification protocol of AamA (also pGEX-6P-3) modified after Blaschke et al. [6]. In further studies, parameters would have to be adjusted to increase the expression level.

Table showing single steps of RibD purification. For protein purification a 200 ml *E. coli* culture was used. The weight of the wet pellet was 2 g. Purity of RibD was calculated with the ImageJ program.

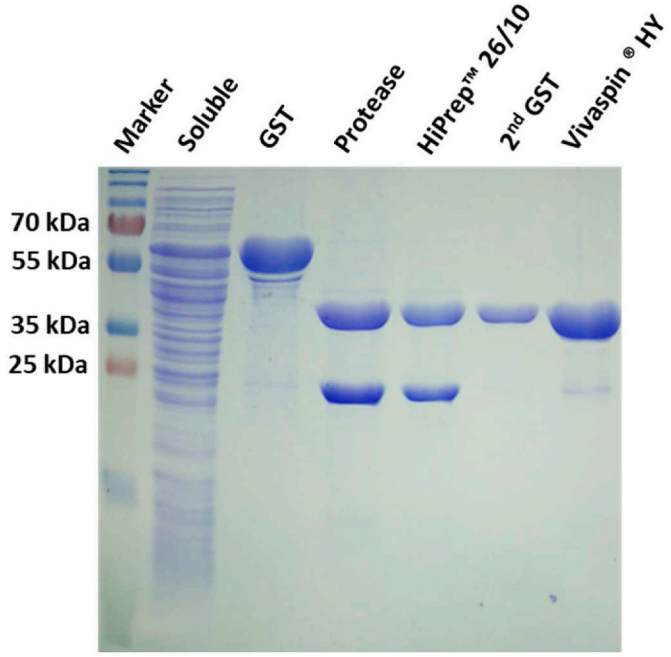

Fig. 6. Purification of Pyrimidine Deaminase RibD (A1S_0221):
Sodium-dodecyl-sulfate (SDS) gel representing single steps of Pyrimidine Deaminase purification, including supernatant after centrifugation of cell-debris (soluble), fusion-protein (GST-RibD) after GSTPrep™ FF 16/10 Column, RibD after cleavage with PreScission protease, RibD after buffer change with HiPrep™ 26/10 Column, RibD after removal of the GST-Tag (GSTPrep™) FF 16/10 and after concentration using a Vivaspin® ultrafiltration unit with a Hydrosart® membrane.

Table 3
Purification table of Pyrimidine Deaminase RibD (A1S_0221).

Purification step	Total Volume [ml]	Protein Conc. [mg/ml]	Total Protein [mg]	Total RibD [mg]	Purity RibD [%]	Purification [fold]
Soluble bacterial lysate	37	2.3	85.1	18.72	22	1
GSTPrep™	10	1.5	15	13.99	93.3	4.2
HiPrep™ 26/10	12	0.78	9.36	4.86	52	2.4
2nd GSTPrep™	12	0.3	3.6	3.5	98.5	4.5
Vivaspin® 15R HY	1.8	1.6	2.88	2.79	97	4.4

5.6. Structural analysis of RibD via small angle X ray scattering (SAXS)

A summary of the RibD SAXS data, p(r) profile and associated models are shown in Fig. 7, while the structural parameters calculated from the data are reported in Supplementary Table 4. After the effects of non-specific aggregate scattering are removed from the very lowest of scattering angles ($s < 0.16$ nm^{-1}), it is possible to conclude that the protein is predominantly dimer in solution (MW = 75–87 kDa; $V_p = 115$ nm^3) that adopts a conformation consistent with the previously solved X-ray crystal structure of a highly homologous *Acinetobacter baumannii* sp. RibD dimer (PDB, 3ZPG; MW = 77 kDa; UniProt: D0CB74) that shares 97% amino acid sequence identity with the RibD used in this study (UniProt: A0A5P1UGY3). The 3ZPG dimer fits the SAXS data with a χ^2 of 1.2, CorMap $p = 0$ (compared to a $\chi^2 = 36$ for the monomer), while an initial RibD dimer homology model, which considers the 3% difference in amino acid sequence with the 3ZPG isoform – but is near structurally identical (RMSD Cα = 0) – also fits the scattering data with a χ^2 of 1.2, CorMap p = 0. The R_g calculated from the SAXS data (3.6–3.65 nm) is also commensurate with the dimer models ($R_g = 3.5$ nm; monomer = 2.4 nm) and the resulting *ab intio GASBOR* DR-models and subsequent *SASREF* or *SREFLEX* atomistic rigid-body models, which fit the SAXS data very well (χ^2 range = 1.07–1.15, CorMap $p = 0.0005$–0.6), are all similar in disposition to the structure of 3ZPG. For example, on comparing the 3ZPG dimer to the *SASREF* or *SREFLEX* refined models, the RMSD Cα falls in the range of 4–8 Å. What the SAXS data might allude to is that the peripheral zinc-binding domains of the protein, that form globular lobes at either end of the dimer, may sample a constrained set of spatial positions relative to the core dimerization domains. However, aside from a tentative suggestion of limited conformational sampling by these peripheral lobes in solution, there are very few global structural differences between the X-ray crystal structure and the SAXS-based models at the nominal resolution of SAXS (~1 nm). SAXS measurements of RibD and AmaA in combination gave no evidence for interaction of both proteins.

6. Results of interaction studies between RibD, NrdR, AcnB and AamA

6.1. Interaction studies between AamA, the DNA fragment nrdR and the NrdR protein using agarose-gel-electrophoresis

To study protein-protein interactions as well as protein-DNA interactions between AamA, the *nrdR* DNA fragment, and the NrdR protein, respectively, an electrophoretic mobility shift assay was performed. Therefore, the *nrdR* gene (including promotor-region) was amplified by PCR. After incubation, samples were applied on an agarose-gel (1.5%). The assay was carried out in a concentration-dependent manner. In this experiment (TBE buffer pH: 8.3) AamA (pI = 9.1) possesses a positive net charge and therefore was expected to run opposed to the DNA. Therefore, the comb was inserted in the middle of the gel. Results are shown in Fig. 8. Proteins NrdR and AamA are not visible when they were applied alone. In the case of AamA combined with the *nrdR* fragment, free DNA decreased with increasing AamA suggesting a DNA binding activity of AamA. By contrast, NrdR exhibits no DNA binding activity when it is incubated with *nrdR*. Assays with a small amount of AamA (0.5 μg) and a concentration serious of NrdR (1.0, 5.0 and 10.0 μg) in combination with *nrdR* DNA also yielded no mobility shift (data not shown). Note that DNA/AamA complexes are barely visible in the gel because they stick to the slots used for sample loading. Moreover, the AamA nucleic acid binding activity was also tested with other DNA fragments (*rrF2*, *gst*) and was found to be independent of the sequence (**S. 5**).

6.2. Restriction-protection-assay with AamA and purified proteins

The restriction-protection assay was carried out to investigate if the suspected protein interaction partners have an effect on the methyltransferase activity of AamA. Therefore, AamA was incubated together with the purified AcnB monomer fraction and RibD. As control BSA was used. As substrate the gene segment Int1 (800 bp) carrying one AamA-specific target site was used. After 20 min of incubation with AamA, Int1 was partially protected from restriction with *EcoRI*. After 40 min, AamA-specific methylation provided complete protection. When other proteins were added to the assay, the methyltransferase activity of AamA was slightly reduced (Fig. 9). This is the case for RibD and AcnB but also for BSA suggesting a molecular crowding effect rather than specific protein/protein interactions.

Beside these illustrated results of various interaction studies between AamA and potential interaction partners (RibD, AcnB and NrdR), we implemented additional biochemical methods (Supplementary Table 1). However, BN-PAGE (S. 1, S. 2), EMSA (S. 3), co-immunoprecipitation (S. 4) and chemical crosslinking provided no evidence of an interaction between AamA and proteins purified in this work.

7. Discussion and conclusion

In this study we recombinantly produced selected proteins to examine possible interactions with AamA, which in former studies had

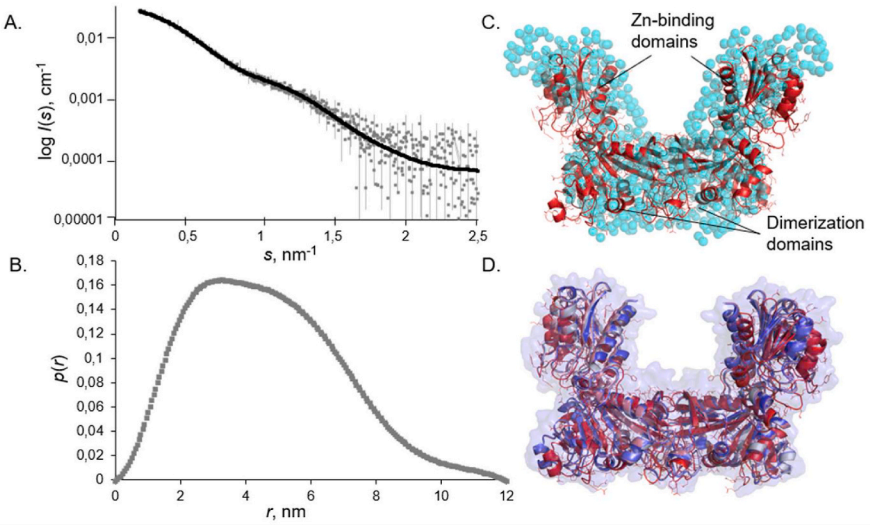

Fig. 7. SAXS data and modelling of RibD:
A. RibD SAXS data (grey squares) and a representative model fit example (black line refers to panel D). **B.** The corresponding *p(r)* profile of real-space distance frequency. **C.** Spatial overlay of a GASBOR DR-model (Cyan-spheres) with the previously determined X-ray crystal structure, PDB: 3ZPG (red ribbons; $\chi^2 = 1.2$). **D.** A spatial alignment of *SASREF* and *SREFLEX* rigid-body model examples of RibD (blue ribbons, $\chi^2 = 1.1$) showing only minor movements in the Zn-binding modules relative to the X-ray crystal structure. Additional models and fits maybe locates under the SASBDB accession code SASDNC5.

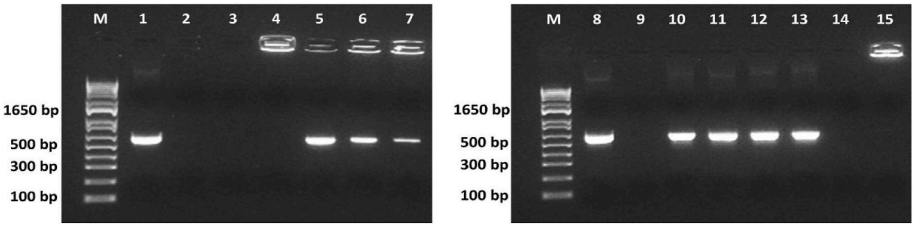

Fig. 8. Concentration-dependent interaction studies between AamA and the NrdR protein/*nrdR* gene by using Electrophoretic mobility shift assay (EMSA) performed on an agarose-gel:
1.5% Agarose-gel with GelRed™ (1:10.000) staining showing applied samples:
Marker (M): 1 Kb Plus DNA Ladder, (1): amplified *nrdR* (285 ng) gene, (2): AamA (5 μg), (3): NrdR (10 μg),
(4): NrdR (10 μg) with AamA (5 μg) and *nrdR* (285 ng), (5): AamA (0.5 μg) with *nrdR* (285 ng), (6): AamA (1.0 μg) with *nrdR* (285 ng), (7): AamA (2.0 μg) with *nrdR* (285 ng), (8): amplified *nrdR* (285 ng) gene,
(9): NrdR (10 μg), (10): NrdR (0.5 μg) with *nrdR* (285 ng), (11): NrdR (1.0 μg) with *nrdR* (285 ng), (12): NrdR (5.0 μg) with *nrdR* (285 ng), (13): NrdR (10.0 μg) with *nrdR* (285 ng), (14): AamA (5 μg), (15): AamA (5 μg) with *nrdR* (285 ng).

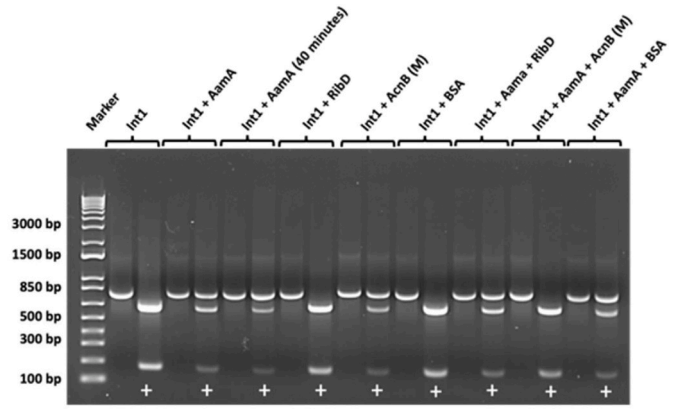

Fig. 9. Methylation assay between Int 1 and AamA together with RibD, AcnB (M) and BSA with subsequent restriction analyses by using EcoRI digestion:
Protection of the Int1 (1 μg) fragment against digestion with EcoRI restriction enzyme was analyzed after performing a methylation assay with AamA alone or in combination with proteins RibD, AcnB (M) and BSA. Therefore, samples were incubated for 20 min at 37 °C. As a control AamA together with Int1 was also incubated for 40 min. After this time AamA is fully saturated. Afterwards AamA was inactivated at 95 °C and samples were purified with a PCR purification kit. Finally, Int1 fragments were cut with the EcoRI restriction enzyme (lines with white crosses) and samples were applied to an 1.5% agarose gel. Marker: 1 kb Plus DNA Ladder.

shown a very low specific activity (Blaschke et al., 2018). We thus hypothesized that interaction partners could help AamA to find its target methylation site within the genome. By first performing a pulldown assay and by exploring the genomic surrounding of the *aamA* gene, we selected the bifunctional aconitate hydratase 2/2-methylisocitrate dehydratase AcnB, the putative transcriptional repressor NrdR and the pyrimidine deaminase/reductase RibD as possible interaction partners. Purification of proteins AcnB, NrdR and RibD could be established in the milligram-scale. In the case of AcnB, aggregation tendency could be suppressed by adding the reducing agent DTT, and by performing size exclusion chromatography, aggregate, dimer, and monomer fractions of AcnB were separated. For structural analyses of AcnB, RibD and NrdR, SAXS measurements were performed alone and in combination with AamA. For RibD and AcnB, solution structure models could be generated on the basis of SAXS data. In the case of RibD, the crystal structure of which has already been studied by Dawson et al. [7], the solution structure was determined and compared. The generated model also shows a dimer in solution with an estimated molecular mass of 75–87 kDa. Furthermore, the dimer consists of two units each harboring a reductase and a deaminase active site. All in all, there are only a few differences between the protein in solution and the crystalline form. In the case of AcnB, the monomer and dimer fractions which were separated performing size exclusion chromatography were measured by SAXS. In comparison to the crystal structure of *E. coli* AcnB, $AcnB_{Ab}$ is very similar. Likewise, $AcnB_{Ab}$ possesses an N-terminal HEAT, a middle-cap, and a C-terminal cup domain. In comparison to the Alphafold2-prediction model and the *E. coli* homologue model, the domain conformation of $AcnB_{Ab}$ is more open. The reason for this could be the ability of $AcnB_{Ab}$ to form multiple structural states. Furthermore, the evaluation of an exact solution model was made more difficult because of the $AcnB_{Ab}$ dimer fraction. While we could still create solution structure models for RibD and AcnB, this was not possible for NrdR. According to the SAXS data, NrdR forms very large macromolecule (<500+ kDa) assemblies with a long, rod-shaped structure rather than unspecific aggregates. However, NrdR is the only protein which showed a significant change when it was measured together with AamA. By adding AamA to NrdR, the macromolecular structure disassembles into smaller particles with a polydisperse character. All in all, this is the strongest evidence for an interaction partner of AamA so far. This observation also fits very well with the genetic vicinity of *aamA* and *nrdR* genes in the *A. baumannii* genome. However, we need to consider some limitations when interpreting this observation. NrdR is known as a Zn finger/ATP cone protein [8]. In this work, we purified NrdR as a His-tagged protein so that the zinc ions might have been lost during Ni affinity. This might have resulted in the formation of macromolecular assemblies of NrdR as well as in a loss of nucleic acid binding activity. Moreover, the His-tag itself might have promoted macromolecular assembly. The effect that was visible in the SAXS data showing disassembly of NrdR macromolecules into smaller particles after addition of AamA could thus also be explained by AamA-induced shielding of such possible His-tag interactions. Future studies will include the production of tag-free NrdR and multivariate interaction studies including low molecular weight compounds such as Zn^{2+}, ATP, SAM etc. as well as concentration-dependent SAXS analyses. Beside the results of the SAXS analysis, interactions between AcnB, NrdR, RibD and AamA were also studied using biochemical methods such as BN-PAGE, chemical cross linking and EMSA (Supplementary Table 1). However, these preliminary approaches provided us with no evidence of interactions between AamA and purified proteins. Further, we could point up the binding behavior of AamA while binding to DNA fragments of *nrdR* in a concentration-dependent manner (Fig. 8). From a paper by Kröger et al. (2018) [40] we know that *aamA* and *ribD* are co-expressed in *A. baumannii* strain ATCC 17978. By contrast, our results suggest that *aamA* as well as the *ribD* are each expressed monocistronically in *A. baumannii* strain 29D2 (S. 6). To characterize AamA-dependent DNA methylation as a potential epigenetic control mechanism in *A. baumannii*, modification-specific genome analyses are underway.

Author statement

Kristin Weber: Conceptualization; Investigation; Methodology; Visualization; Data curation; Writing - original draft, Joerg Doellinger: Investigation; Methodology; Data curation; Writing - original draft, Cy M. Jeffries: Investigation; Methodology; Visualization; Data curation; Writing - original draft, Gottfried Wilharm: Conceptualization; Funding acquisition; Supervision; Validation; Project administration; Writing - review & editing.

Acknowledgement

This work was funded by the Deutsche Forschungsgemeinschaft (DFG) within FOR 2251 (Grant No. WI 3272/3-2).

Appendix A. Supplementary data

Supplementary data to this article can be found online at https://doi.org/10.1016/j.pep.2022.106134.

References

[1] A.J. Berdis, et al., A cell cycle-regulated adenine DNA methyltransferase from Caulobacter crescentus processively methylates GANTC sites on hemimethylated DNA, Proc. Natl. Acad. Sci. U. S. A. 95 (6) (1998) 2874–2879.
[2] L.S. Kahng, L. Shapiro, The CcrM DNA methyltransferase of Agrobacterium tumefaciens is essential, and its activity is cell cycle regulated, J. Bacteriol. 183 (10) (2001) 3065–3075.
[3] J. Casadesús, D. Low, Epigenetic gene regulation in the bacterial world, Microbiol. Mol. Biol. Rev. 70 (3) (2006) 830–856.
[4] J.R. Horton, et al., Structures of Escherichia coli DNA adenine methyltransferase (Dam) in complex with a non-GATC sequence: potential implications for methylation-independent transcriptional repression, Nucleic Acids Res. 43 (8) (2015) 4296–4308.
[5] M.G. Marinus, A. Løbner-Olesen, DNA methylation, EcoSal Plus 6 (1) (2014).
[6] U. Blaschke, et al., Recombinant production of A1S_0222 from Acinetobacter baumannii ATCC 17978 and confirmation of its DNA-(adenine N6)-methyltransferase activity, Protein Expr. Purif. 151 (2018) 78–85.
[7] A. Dawson, et al., Structure of diaminohydroxyphosphoribosylaminopyrimidine deaminase/5-amino-6-(5-phosphoribosylamino)uracil reductase from Acinetobacter baumannii, Acta Crystallogr., Sect. F: Struct. Biol. Cryst. Commun. 69 (Pt 6) (2013) 611–617.
[8] I. Grinberg, et al., The Streptomyces NrdR transcriptional regulator is a Zn ribbon/ATP cone protein that binds to the promoter regions of class Ia and class II ribonucleotide reductase operons, J. Bacteriol. 188 (21) (2006) 7635–7644.
[9] D.A. Rodionov, M.S. Gelfand, Identification of a bacterial regulatory system for ribonucleotide reductases by phylogenetic profiling, Trends Genet. 21 (7) (2005) 385–389.
[10] I. Grinberg, et al., Functional analysis of the Streptomyces coelicolor NrdR ATP-cone domain: role in nucleotide binding, oligomerization, and DNA interactions, J. Bacteriol. 191 (4) (2009) 1169–1179.
[11] N. Dreux, et al., Correction for Dreux et al., Ribonucleotide Reductase Repressor NrdR as a Novel Regulator for Motility and Chemotaxis during Adherent-Invasive Escherichia coli Infection, Infect. Immun. 83 (10) (2015) 4174.
[12] S. Banerjee, et al., Iron-dependent RNA-binding activity of Mycobacterium tuberculosis aconitase, J. Bacteriol. 189 (11) (2007) 4046–4052.
[13] L. Cunningham, M.J. Gruer, J.R. Guest, Transcriptional regulation of the aconitase genes (acnA and acnB) of Escherichia coli, Microbiology (Read.) 143 (Pt 12) (1997) 3795–3805.
[14] M.W. Hentze, L.C. Kühn, Molecular control of vertebrate iron metabolism: mRNA-based regulatory circuits operated by iron, nitric oxide, and oxidative stress, Proc. Natl. Acad. Sci. U. S. A. 93 (16) (1996) 8175–8182.
[15] P.A. Jordan, et al., Biochemical and spectroscopic characterization of Escherichia coli aconitases (AcnA and AcnB), Biochem. J. 344 Pt 3 (Pt 3) (1999) 739–746.
[16] C.M. Marcos, et al., The multifaceted roles of metabolic enzymes in the Paracoccidioides species complex, Front. Microbiol. 5 (2014) 719.
[17] Y. Tang, et al., Escherichia coli aconitases and oxidative stress: post-transcriptional regulation of sodA expression, Microbiology (Read.) 148 (Pt 4) (2002) 1027–1037.
[18] S. Liu, et al., Production of riboflavin and related cofactors by biotechnological processes, Microb. Cell Factories 19 (1) (2020) 31.
[19] S. Bereswill, et al., Molecular analysis of riboflavin synthesis genes in Bartonella henselae and use of the ribC gene for differentiation of Bartonella species by PCR, J. Clin. Microbiol. 37 (10) (1999) 3159–3166.
[20] G. Richter, et al., Biosynthesis of riboflavin: cloning, sequencing, mapping, and expression of the gene coding for GTP cyclohydrolase II in Escherichia coli, J. Bacteriol. 175 (13) (1993) 4045–4051.
[21] H. Blum, H. Beier, H.J. Gross, Improved silver staining of plant proteins, RNA and DNA in polyacrylamide gels, Electrophoresis 8 (2) (1987) 93–99.
[22] A. Shevchenko, et al., In-gel digestion for mass spectrometric characterization of proteins and proteomes, Nat. Protoc. 1 (6) (2006) 2856–2860.
[23] Y. Ishihama, J. Rappsilber, M. Mann, Modular stop and go extraction tips with stacked disks for parallel and multidimensional Peptide fractionation in proteomics, J. Proteome Res. 5 (4) (2006) 988–994.
[24] C. Fillebeen, N. Wilkinson, K. Pantopoulos, Electrophoretic mobility shift assay (EMSA) for the study of RNA-protein interactions: the IRE/IRP example, JoVE (94) (2014).
[25] C.E. Blanchet, et al., Versatile sample environments and automation for biological solution X-ray scattering experiments at the P12 beamline (PETRA III, DESY), J. Appl. Crystallogr. 48 (Pt 2) (2015) 431–443.
[26] D. Franke, A.G. Kikhney, D.I. Svergun, Automated acquisition and analysis of small angle X-ray scattering data, Nucl. Instrum. Methods Phys. Res. Sect. A Accel. Spectrom. Detect. Assoc. Equip. 689 (2012) 52–59.
[27] A. Guinier, La diffraction des rayons X aux trčs petits angles: application ą l'étude de phénomčnes ultramicroscopiques, Annales de physique, 1939.
[28] D. Svergun, Determination of the regularization parameter in indirect-transform methods using perceptual criteria, J. Appl. Crystallogr. 25 (4) (1992) 495–503.
[29] D.I. Svergun, Restoring low resolution structure of biological macromolecules from solution scattering using simulated annealing, Biophys. J. 76 (6) (1999) 2879–2886.
[30] D.I. Svergun, M.V. Petoukhov, M.H. Koch, Determination of domain structure of proteins from X-ray solution scattering, Biophys. J. 80 (6) (2001) 2946–2953.
[31] M.V. Petoukhov, et al., Reconstruction of quaternary structure from X-ray scattering by equilibrium mixtures of biological macromolecules, Biochemistry 52 (39) (2013) 6844–6855.
[32] J. Jumper, et al., Highly accurate protein structure prediction with AlphaFold, Nature 596 (7873) (2021) 583–589.
[33] C.H. Williams, et al., E. coli aconitase B structure reveals a HEAT-like domain with implications for protein-protein recognition, Nat. Struct. Biol. 9 (6) (2002) 447–452.
[34] M.V. Petoukhov, D.I. Svergun, Global rigid body modeling of macromolecular complexes against small-angle scattering data, Biophys. J. 89 (2) (2005) 1237–1250.
[35] A. Panjkovich, D.I. Svergun, Deciphering conformational transitions of proteins by small angle X-ray scattering and normal mode analysis, Phys. Chem. Chem. Phys. 18 (8) (2016) 5707–5719.
[36] D. Svergun, C. Barberato, M.H. Koch, CRYSOL–a program to evaluate X-ray solution scattering of biological macromolecules from atomic coordinates, J. Appl. Crystallogr. 28 (6) (1995) 768–773.
[37] D. Franke, et al., ATSAS 2.8: a comprehensive data analysis suite for small-angle scattering from macromolecular solutions, J. Appl. Crystallogr. 50 (Pt 4) (2017) 1212–1225.
[38] D. Franke, C.M. Jeffries, D.I. Svergun, Correlation Map, a goodness-of-fit test for one-dimensional X-ray scattering spectra, Nat. Methods 12 (5) (2015) 419–422.
[39] A.G. Kikhney, et al., SASBDB: towards an automatically curated and validated repository for biological scattering data, Protein Sci. 29 (1) (2020) 66–75.
[40] C. Kröger, et al., The primary transcriptome, small RNAs and regulation of antimicrobial resistance in Acinetobacter baumannii ATCC 17978, Nucleic Acids Res. 46 (18) (2018) 9684–9698.